Geolocalization of water-waves origin within water distribution networks using time reversal of first event detection

Romain Guibert, Alexandre Bayle, Franck Plouraboué

Geolocalization of water-waves origin within water distribution networks using time reversal of first event detection

R. Guibert, A. Bayle and F. Plouraboué

Institut de Mécanique des Fluides de Toulouse, IMFT, Université de Toulouse, CNRS, Toulouse, France

Abstract

Drinking water distribution networks in urban areas are daily ~~-based~~ subject~~ed~~ to fast propagating pressure waves resulting from routine operations. These water-hammer waves lead~~s~~ to structural aging and facility damages, the origin of which is not easy to find ~~,~~ but are sometimes of high managerial interest. In this contribution, we demonstrate that using a reasonable number of high-frequency pressure detectors distributed within the network combined with a proper post-processing method permits a close geolocalization of the damaging wave origin. The method is first tested and validated on a real water distribution network having approximately 26 000 pipes, whereas considering a known, prescribed wave~~-~~origin, so that the sensitivity to sensor number (sensor spatial density), sensor location and signal-to-noise ratio on the geolocalization robustness ~~is~~ are analyzed in detail. It is then applied and illustrated over real sensor recordings the result of which are validated on the field from history matching. This paper thus presents the first field-scale geolocalization of water-hammer events origin test as well conditions for which, given sensor density and signal-to-noise ratio, the geolocalization success is to be expected.

Keywords: water distribution network, water-hammer, high-frequency detector, geolocalization

2010 MSC: 00-01, 99-00

1. Introduction

Water hammer waves within Water Distribution Networks (WDNs) are a common hindrance resulting from many possible routine operations, either organized, vol~~o~~untary or accidental. Not only these waves are responsible ~~of~~ for structure~~'s~~ wear, but they are also capable of facility damage~~s~~. Intermittent water supply operations have indeed been correlated to incident damages in WDNs (Agathokleous and Christodoulou, 2016).

Since the water-hammer wave speed in WDNs is very fast (between ~~700~~ for 350 m/s for the softest plastic pipes to 1200 m/s for cast iron pipes ~~depending on pipes' mechanical properties~~) having a rather slow attenuation, the wave generated at a given location can propagate over a large portion of the entire urban

⋆Fully documented templates are available in the elsarticle package on CTAN.

networks within a few seconds before decaying in less than a minute. It results in a myriad of reverberation causing as much disorder and possible breakages as pre-existing weaknesses. Since the life-time of these events inside the network is short, and since they are not numerous within a day (e.g less than a few per day in the considered city of about half a million people), the dynamic of each water-hammer event can be considered separately. Being able to find the origin of a cascade of reverberating water-waves events is interesting from various viewpoints: patrimonial management, security, insurances, etc...

Nevertheless, this topic has not been developed in real WDNs because it necessitates to overcome overcoming several challenges, not been fully addressed yet. Firstly, urban WDNs are, in many cases, not sufficiently and reliably detected and observed in details for a precise modeling of transient waves into them to be relevant. Secondly, localizing the origin of water-hammer waves necessitates a real-time high-frequency monitoring with widely distributed detectors, rarely deployed in WDNs. Thirdly, the computational cost of direct transient wave modeling in water distribution networks is very challenging either using the Method Of Characteristics (Wang et al., 2014; Nault et al., 2018; Meniconi et al., 2021; Moosavian and Lence, 2020; Riaño-Briceño et al., 2022), or finite volumes e.g (Pal et al., 2021; Zhang et al., 2021). Fourthly, an inverse method capable of identifying the origin of a reverberating water hammer wave over a large network, solving as many direct problems as tentative tries for possible origin, is obviously even more challenging. Last but not least, from a more fundamental viewpoint, even if the uniqueness of the wave origin from detecting reverberation waves has been established on discrete wave models on arbitrary networks (Caputo et al., 2019; Plouraboué et al., 2022), it is still a pending issue for continuum ones.

Hence, even if the idea of using the entire time-course of signal reverberation within the network at the sensor location so as to enlarge as much as possible data collection is appealing, in practice, this approach is still very difficult to develop at the present state of the art (Che et al., 2021). As part of the European "Surge-Net" project, Ferrante et al. (2009) carried out leakage location tests using echo analysis, by combining Lagrangian and wavelet transforms signal analysis, in the Lintrahen's (Scotland) WDN main trunk. Shucksmith et al. (2012) performed leakage tests on the Bradford's (Yorkshire, UK) WDN. The authors operated at the neighbourhood scale (about 100m of weakly branched pipe) using spectral analysis for the leak echo-localization (cepstrum analysis) and with a wide variety of pipe materials (PVC, cast iron, asbestos–cement). Recently, Meniconi et al. (2015) also combined a wavelet transform analysis with a Lagrangian method to preliminary examine one of the main pressure transimission lines of the Milan's (Italy) WDN. Although achievable on a district scale or on the main supply pipes of a water distribution network, the implementation of such leak detection techniques is questionable for large-scale analysis. Indeed, techniques based on leak wave reflection suffer from a high sensitivity to propagation speed uncertainties and surrounding noise (Wang et al., 2021). Moreover, an idealized test case without leakage or blockage is required for allowing direct comparison with the field pressure signal. Recently, Meniconi and co-workers

have performed such measurements on a laboratory network (Meniconi et al., 2022a,b). However, such benchmark case is often not operationally possible or~~, alternatively~~ prone to mode~~l~~ling errors (e.g. cross-section pressure interactions, wave attenuation, incorrect network topology, etc...) as in other contexts such as quality event detection (Kessler et al., 1998).

This is why an approximate alternative method avoiding the cost of a complete time-course of wave propagation evaluation is proposed and develo~~p~~ped in this contribution. Rather than trying to exploit the entire signal complexity recorded at each sensor location, we take advantage of the first arrival time only. This already permits ~~to~~ back-track ~~the~~ wave origin using a time-reversal method. Time reversal methods, either at the individual pipe level (Grigoropoulos et al., 2021) or at the network one (Shen et al., 2016) have already permit computationaly efficient source identification. This method has been used to develop noise-tolerant pipeline defect detection (Wang and Ghidaoui, 2018; Wang and Xie, 2018; Meniconi et al., 2021) in the precise context of water-hammer waves. ~~The aim of this contribution is~~ This contribution aims to demonstrate that combining first-event detection with time-reversal is an interesting strategy to geolocalize water-hammer events in real WDN.

The paper is organized as follows. Section 2.1 describes the material related to the urban network and the pressure sensors used within the study. Section 2.2 details the algorithm of the first event detection, time reversal method, and candidate order~~ing~~. Section 3.1 discusses the localization of prescribed events in a real WDN ~~so as~~ to test and validate the method efficiency and its sensitivity to detectors number (more precisely the sensor "density", the sensor number divided by the total node number in the network). Section 3.2 finally describes the application of the proposed method to the field's data ~~so as~~ to geolocalize real events and discuss the obtained results.

2. Materials and Methods

2.1. Materials

The materials consist in ~~a~~ WDN data within which high-frequency pressure detectors are disposed of.

2.1.1. Water distribution network data

The entire network from the city of Toulouse (France) illustrated in figure 1a is composed of a total of 26 094 pipes. It has been formatted in Epanet format providing the pipe lengths, structural properties and diameters. The distinct pipe's composition within the network is detailed in table 1, showing a great majority of cast iron material. The heterogeneity of pipe diameters and lengths is illustrated in figure 1b and c showing a great diversity of diameter and length over more than a decade.

Material	**Quantity (%)**	**Length (%)**
Iron	87.66	89.28
Steel	1.97	4.04
PVC	1.01	1.22
Others	2.15	1.46
Unknown	7.21	4.00

Table 1: Distribution of pipe materials. Others materials are inox, fiber, PE, and PVD.

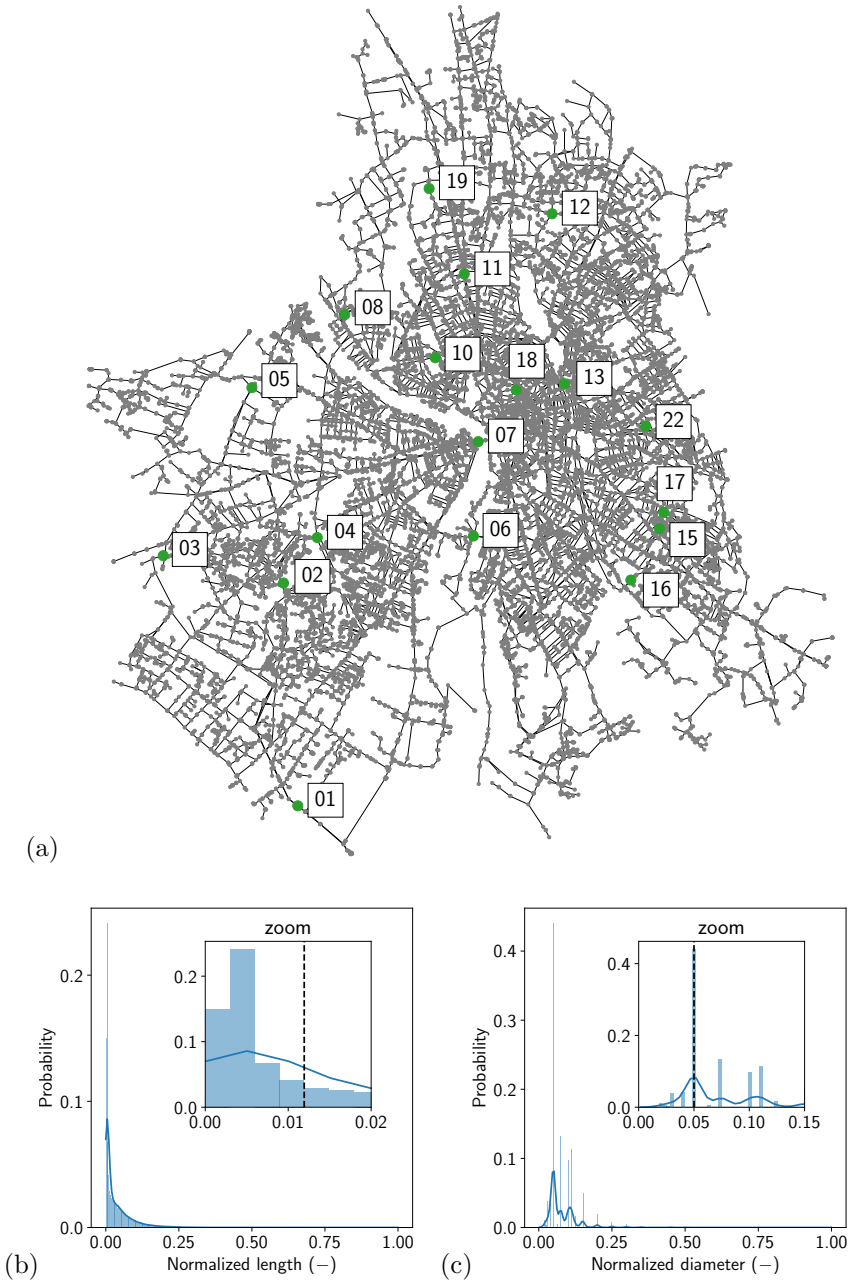

Figure 1: (a) Topography of the considered water distribution network. The network is composed of 23 784 nodes, 26 094 pipes for a total pipe distance close to 1 200 km. The positions of high-frequency pressure detectors (from 1 to 18), arranged within the network are illustrated with green dots. (b) Probability Density Functions (PDF) (with the corresponding histogram in zoom's inset) of dimensionless lengths (median 0.012 indicated with vertical dotted lines) normalized by maximal length. (c) same as (b) for dimensionless diameters (median 0.05) normalized with maximal diameter.

This result in wave-propagation heterogeneity to be taken care-off ~~from~~ of considering the adapted velocity in

each pipe. Local wave-hammer wave velocity indeed depends on the pipe diameter, length, thickness, Young modulus, and material density. It is estimated from known validated formulas (cf Appendix). Furthermore, the chosen location for high-frequency pressure sensor~~'~~s (18 in total) is depicted in Figure 1a with green dots, each described by a label between 1 to 18, being spatially uniformly distributed over the urban network.

2.1.2. High-frequency pressure detectors

Pressure detectors record at 128 Hz frequency with a $5000Pa$ accuracy. The recording mode is triggered by an awaking threshold which empirically sets from the base signal. This precautionary procedure avoids recording embarrassing irrelevant signal series in the detection event database. Since the event amplitude is expected within the range of $[0.8, 2]10^5$Pa, the relative precision on the detected peak amplitude is of the order of 6.25%. Also, only the time-arrival of the first peak is critical for the chosen method. Each detector has been primarily submitted to a pressure calibration test using a prescribed static pressure before field deployment. Each sensor has its own embarked battery and RAM. Once triggered to awaken mode, the detectors acquire at full high-frequency (i.e. 128Hz) during 300 seconds. The resulting collected data are then ~~more lately~~ transmitted latelly with a standard GSM 3G protocol keeping each signal associated with each detector identifier.

2.2. Methods

The method decomposes into various steps : (i) first event detection into each detectors, (ii) back-propagation from detectors to potential source of detected event using the time-reversal method and (iii) calibration of time-reversal method on the network and detector set. The methods associated with these three steps are now detailed. An additional noise sensitivity check of the method has also been used, the details of which is also given in 2.2.3.

2.2.1. First event detection and time reversal method

First event detection is performed using offline change point detection method (Truong et al., 2020). The detection criteria ~~is~~are associated with a functional minimization associated with the local gradient of the noisy signal. More precisely we use a binary change point detection to perform a fast signal segmentation, coupled with a L^2 cost function that detects mean-shifts in the signal. The determination of the arrival times is illustrated for a real signal in figure 2.

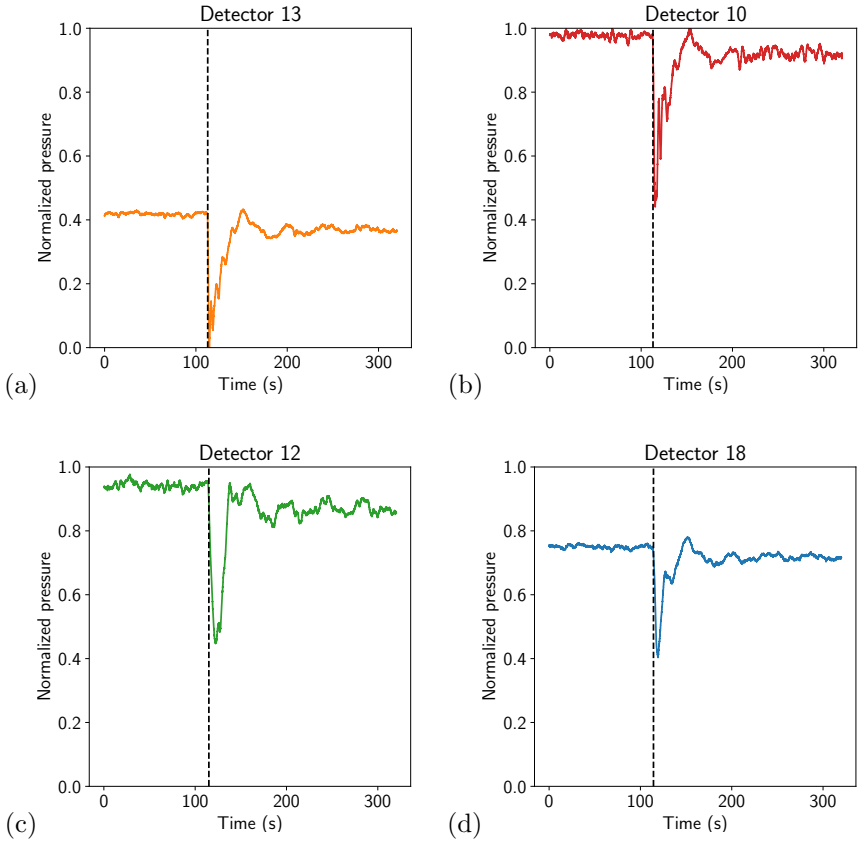

Figure 2: Illustration of change point detection applied to a real pressure signal detected on the considered WDN (figure 1a) using high-frequency detectors. The illustrated event is discussed in subsection 3.2. For each signal related to the event, the normalized pressure is reported versus time (cf figure 7). The obtained arrival time is represented by the vertical dashed line. The signal is captured almost simultaneously at detectors #13 and #10 (respectively at time 112.92 and 112.96 s), then at detector #12 (at time 114.29 s), and finally at detector #18 (115.00 s).

Time- reversal of first event detection within the network follows the approach proposed in Shen et al. (2016). The method principle is detailled in Figure 3. As a prerequisite, each pipe is associated with a time propagation resulting from computing the ratio between pipe length and velocity evaluated following the Appendix formula. Then the signal processing starts when an event has been detected, resulting in a first-time arrival (denoted t_i, $i = 1, 2, 3$ in figure 3a) of the signal at various awaken detectors (denoted d_i, $i = 1, 2, 3$). For each pair of detector/non-detector nodes in the network, a total-time is evaluated from by computing the sum of each time propagation within each pipes along the shortest path between those within the network, as depicted in figure 3b. Performing this total time of propagation between each node and one detector results in the detector back-propagation cartography depicted in figure 3c for detector d_1, figure 3d for detector d_2 and figure 3e for detector d_3. Now using the first-time arrival component vector

t_i, $i = 1, 2, 3$, results in back-propagating-time vectors at each node~~s~~ (each time is colored with the same color as the detector with which it is associated in figure 3f). In Shen et al. (2016) the source node is the one with minimum variance back-propagating-time vector as illustrated in figure 3f. Note, however, that depending on the recorded time, several source nodes are possibly found with this method as depicted in figure 3e. Hence, in the case of noisy recordings one can infer that, in this case, the true source might not necessarily be the one having the minimum variance. Hence, ~~in order~~ to give more robustness to the method (but ~~obviously~~ less sensitivity) we extend the search for the true source ~~from~~by considering the sorted list of back-propagating-time vector variances ~~in order~~ to find the "best" source candidates. This sorted list has to be closed, keeping with a "reasonable" number of possible candidates. This is what we call the method "calibration" as detailed in the next section.

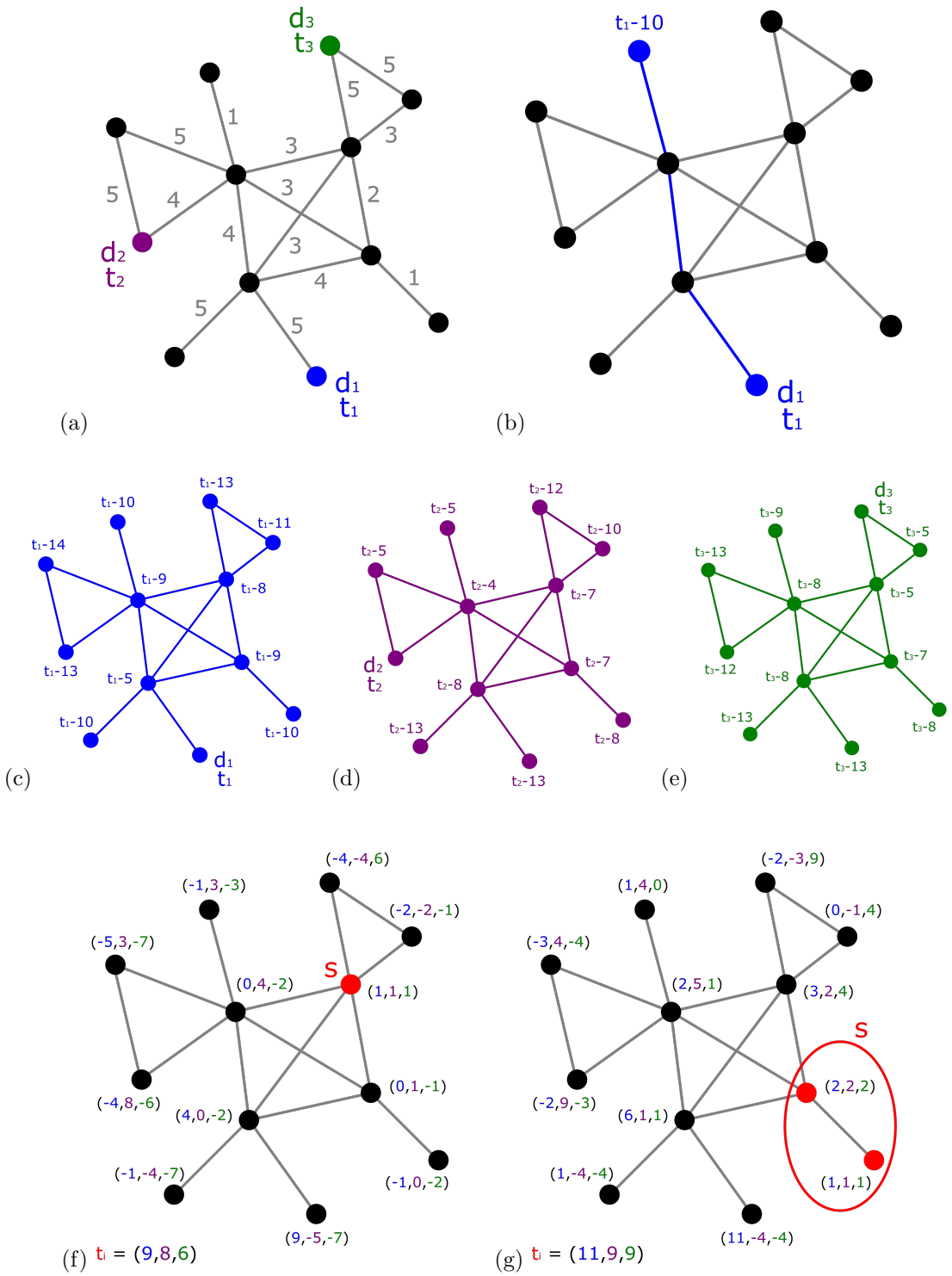

Figure 3: Time-reversal propagation method principle. (a) awaiken detectors d_i, $i = 1, 2, 3$ at first passage time t_i, $i = 1, 2, 3$ (b) Shortest-path between detector d_1 and one node. (c,d,e) Back-propagation cartography for detector d_1-d_2-d_3. (f) For a given arrival time vector, the source node is the one having a back-propagation vector with minimum variance. (g) Depending on the first passage time t_i, the resulting time arrival time vector can lead to several possible source nodes.

2.2.2. Calibration of the time reversal method

In the original research (Shen et al., 2016), the ~~locability~~locality condition is widely discussed. Two main aspects are highlighted: (i) all edge~~s~~ spreading times must be sufficiently different and (ii) nodes with a single neighbor disrupt this condition. Consequently, the success rate (i.e. exact source location) of the method depends on the topology of the considered network and the number of detectors. In our approach, the signals are real and uncertainties necessarily exist in the signal measurements. Moreover, it is currently not possible to deploy sensors on 20% of the nodes in the city networks, as suggested by Shen et al. (2016); the current order of magnitude is less than one percent. In response to this, the method has been adapted to achieve interesting success rates with a limited number of sensors. The resulting variance of each source candidate ~~are~~is sorted ~~in order~~ to produce a tentative hierarchy of the best source candidate. Nevertheless, this priority list is not always relevant: the source having the minimum variance, i.e. the first source in the sorted list of variances, is not always the true source. Hence, a list of potentially successful sources, i.e. "the best choice" among the entire variance list has to be defined. This "best choice" needs a potentially successful source number to be defined. For this, a dedicated "calibration" of the method needs to be performed ~~so as~~ to find the most sensible potentially successful source number. ~~Obviously,~~ This potentially successful source number has to be chosen from a trade-off between *accuracy* and *selectivity*, i.e. maximizing the probability of finding the true source whilst, on the order hand, not increasing too much the number of potential sources. This "calibration" is highly sensitive to the specific network at hand~~s~~, the detector number, and their positions, as well as to the wave velocity variability among the pipes. Hence, this calibration is empirically evaluated using the real network data and the exact detector positions and number~~s~~. For this, we randomly chose sources in the network, perform the time-reversal approach in each case, and built the success-rate histogram of finding the true source at each rank of the variance list. This is what we called the "calibration" of the method.

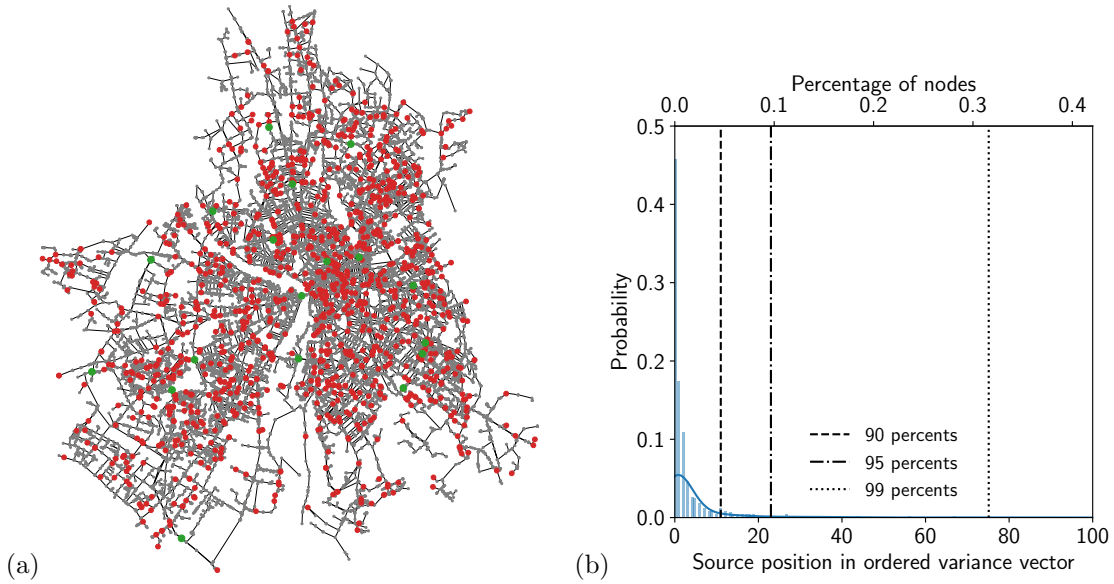

Figure 4: Calibration of the method for the city network and the 18 real sensors (cf. figure 1a). 5% of the network nodes are chosen independently and randomly as sources. (a) network with random sources in red. (b) Calibration histogram and probability density function.

One calibration example is illustrated in figure 4a where all tested sources (used for building statistics) have been colored in red (they represent 5% of the total network). Figure 4b depicts the probability of each candidate ~~to be~~ being a true source versus its rank in the potentially successful source list. The closest to one, the most probable being the true source. Once adding together all potentially successful source probability in the list result in the probability of having the true source versus rank, i.e. versus the chosen potentially successful source number. The 0.9, 0.95, and 0.99 probabilities have been depicted with vertical dotted lines in figure 4b. They are "calibrated" in this case by a potentially successful source number of 11, 23, and 75 respectively.

2.2.3. Time reversal method with noisy data

~~In order t~~To test the influence of noise in the first event detection time, some noise is added to the celerity wave in each pipe. This noise ~~models~~is modeling the uncertainty associated with structural or geometrical parameters both influencing the wave velocity. We chose to impose a multiplicative noise, i.e. a noise being a small fraction of the local value of the wave celerity in each pipe. In this framework, first event detection times become random variables to be evaluated a large number of times ~~in order~~ to access the reliability and sensitivity of the source identification to noise. Obviously, for a given configuration (i.e. fixed network topology, wave celerity field, detector number, and locations) the calibration procedure is performed only once~~,~~ so that for each set of random sources, the noise distribution is applied in a randomly and differently ~~way~~. Increasing the noise amplitude permits ~~to~~ quantifying the degradation of the method performance, ~~so~~

~~as being~~ to be able to extrapolate it for increasing noise and/or uncertainty.

3. Results

3.1. Influence of detector density and signal-to-noise ratio

As discussed in section 2.2.2, the success~~-~~ rate, i.e. the capability of finding the true source among the potentially selected ones depends both upon the sensor spatial density and on the signal-to-noise ratio. We hereby analyze both from randomly chosen detector locations within the network.

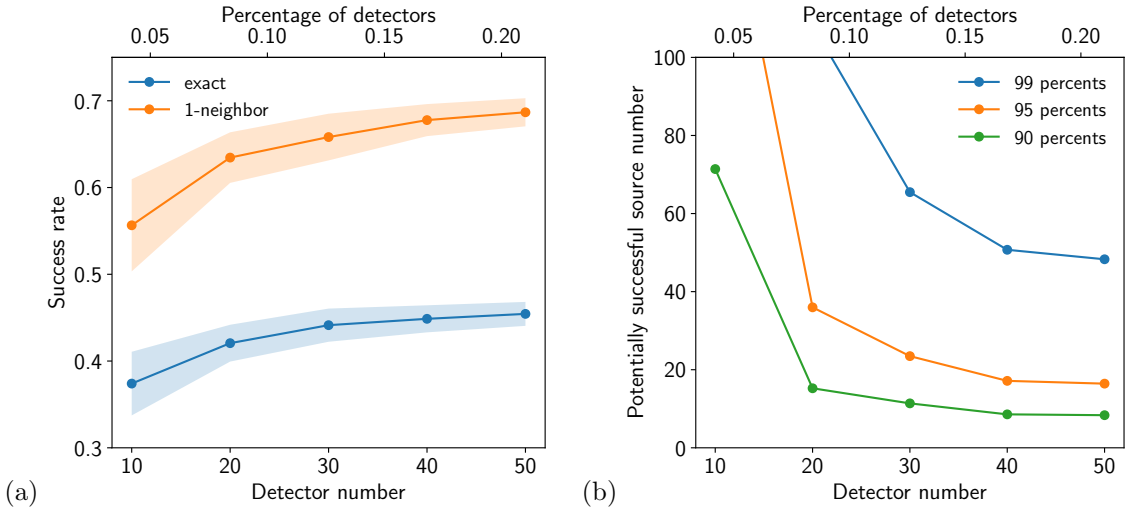

Figure 5: Influence of detector number on the selectivity and success rate of the source geolocalisation. For each detector number, 30 random sets are calibrated, using 5% of temptative randomly chosen true sources among all nodes (1189). (a) Exact and one-neighbor detection ~~versus~~ function of detector number. In each case, the average behavior is plotted with bold continuous lines where respective colored zone displays ± the standard deviation around it. (b) Average values of the potentially successful source number versus detector number.

The detector density influence is first analyzed without noise, i.e. supposing that the wave velocity is perfectly evaluated within each pipe. In this case, 30 randomly chosen detector configurations are analyzed for each varying number of detectors between 10 to 50. This corresponds to a detector "density" (i.e. the percentage of the detector within the total node number of the network) between 0.05% to 0.22%. Note that these detector densities have been voluntarily chosen in a much modest range than the ones tested in Shen et al. (2016), in line with what is currently deployed and what will be deployed ~~in the near future~~ soon. This is motivated by the practical constraint that detectors deployment within the network is costly. Hence it is required to test how the method performs for weak detector density. For such low detector density, it is not expected that the method could provide a highly reliable success rate. Nevertheless, Figure 5a shows

that the success rate associated with the best source in the variance list can reach 45.5% of exact detection for the highest detector density (with 50 detectors). This is already an interesting performance from the practical point of view considering the poor detector deployment effort. Moreover, when relaxing/extending the identification success to a one-neighbor distance within the network, i.e. considering one node distance to the best source of the variance list is a success, then the success rate can reach 68.7% as illustrated in Figure 5a. This means that the obtained geolocalization of the best source positions in the network is useful to locate the true source in its vicinity in case of an unsuccessful search. Hence, it is interesting to relax the *selectivity* of the method (which is the maximum for a single choice associated with the best variance in the potentially successful source list) ~~in order~~ to study how increasing the sensor density with a given calibration (from varying the list success rate from 0.9 to 0.99) impacts its *selectivity*. This calibration sensitivity to detector density ~~are~~ is is shown in figure 5b. Whereas increasing the detector density had a weak impact on the success rate of the best source candidate in the list, on the contrary, one can observe in figure 5b that it has a strong impact on the potentially successful source number which strongly decays as the detector number increases from 10 to 50. This is true for every level of calibration (i.e. for every prescribed success rate from 0.9 to 0.99). Hence, even if the method *accuracy* is poorly sensitive to sensor density, it is *selectivity* is strongly influenced by it. For this reason, we also evaluate the convex hull of potentially successful source~~s~~ positions ~~so as~~ to provide a Region Of Interest (ROI) for the source location. This convex hull is not only useful from the practical viewpoint to delineate the research ROI. It is also useful~~l~~ as a possibly expandable region ~~in order~~ to increase research success, in case of unsuccessful research~~es~~ within it. This convex ~~-~~hull will be exemplified in two practical cases in the next section.

We now turn to the analysis of noise impact on success rate. ~~In order~~ To analyze the expected precision of the geolocalization produced by the first event detection method in the presence of noise, we analyze the performance of the method with the same number of detectors as the one used on the field (18) for a large number of randomly chosen sources when considering a relative uncertainty between 0 to 5% for each local wave velocity in pipes. As expected, the larger the noise amplitude, the lower the success rate. Interestingly enough, the performance degradation scales linearly with the noise amplitude as found in figure 6a and 6b. Hence this permit~~s~~ us to predict the method performances in different contexts for which the uncertainty of the wave velocity ~~are~~ is larger.

3.2. Real events geolocalization

The method is now applied to two real field~~'s~~ data analy~~ic~~s denoted case 1 and case 2. For case 1, figure 7a shows the time variation of the high-frequency pressure signal from the awaken detectors (four of those, # $10, 12, 13, 18$ whose location is given in figure 1) of one event. The geolocalization of the source is provided in figure 7b using various convex-hull of potentially successful source~~s~~ positions associated with various calibration~~s~~ as previously explained in section 3.1. As quantified in table 2, the ROI area provided by

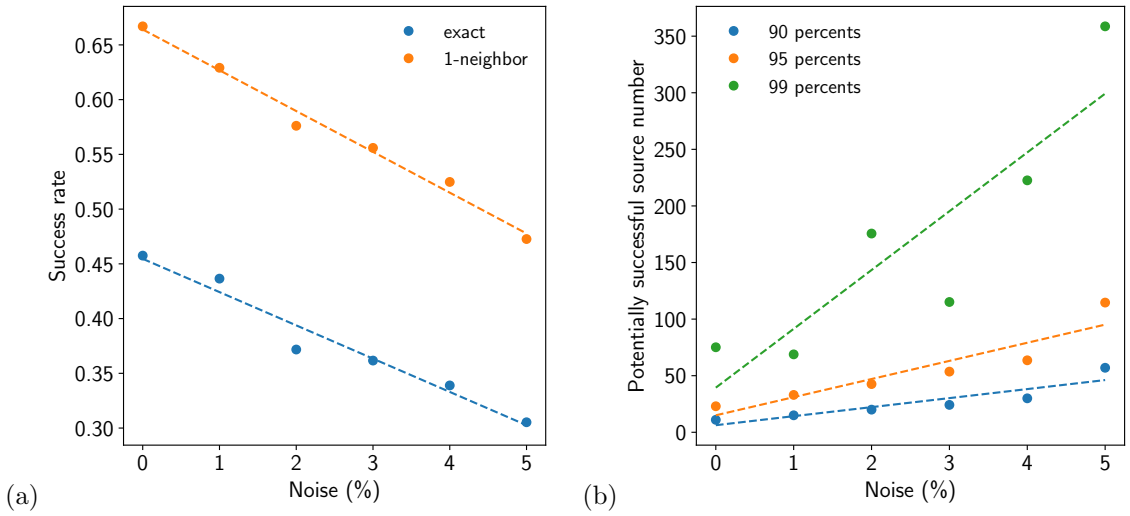

Figure 6: Noise influence on the geolocalization (a) *accuracy* and (b) *selectivity*. Using the 18 detector locations provided in figure 1a, the calibration is performed by randomly adding a multiplicative noise to each pipe travel time, for each tested random source. Evolutions of (a) success rates and (b) potentially successful source number versus noise amplitude. Dashed lines display linear regressions.

the convex hull represents a small fraction (a few percent) of the total network area. ~~Obviously, depending on the calibration level, this area varies.~~ This area varies depending on the calibration level.

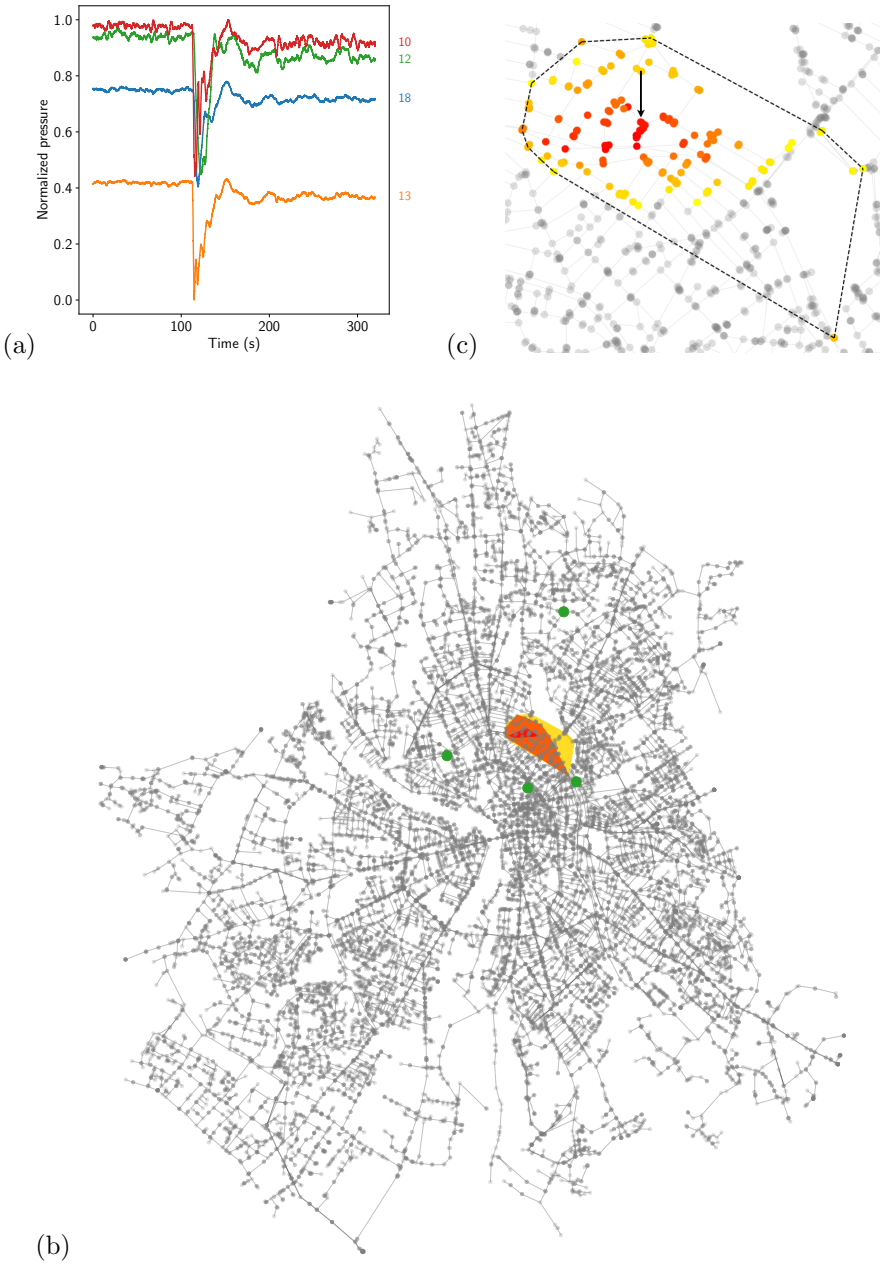

Figure 7: Case 1 illustrating real event detection from the field's data recordings. (a) Normalized pressure signals recorded by high-frequency detectors. (b) Geolocalization of the source with three convex hulls associated with three calibration levels : (yellow) 0.75 %, (orange) 0.5 %, and (red) 0.1 % of potentially successful source number in overall nodes. The four detectors that awaken during this event are depicted in green. (c) Zoom on ROI with the largest hull in dashed lines and nodes colorized versus their variance level from yellow to red for increasing probability of being the source.

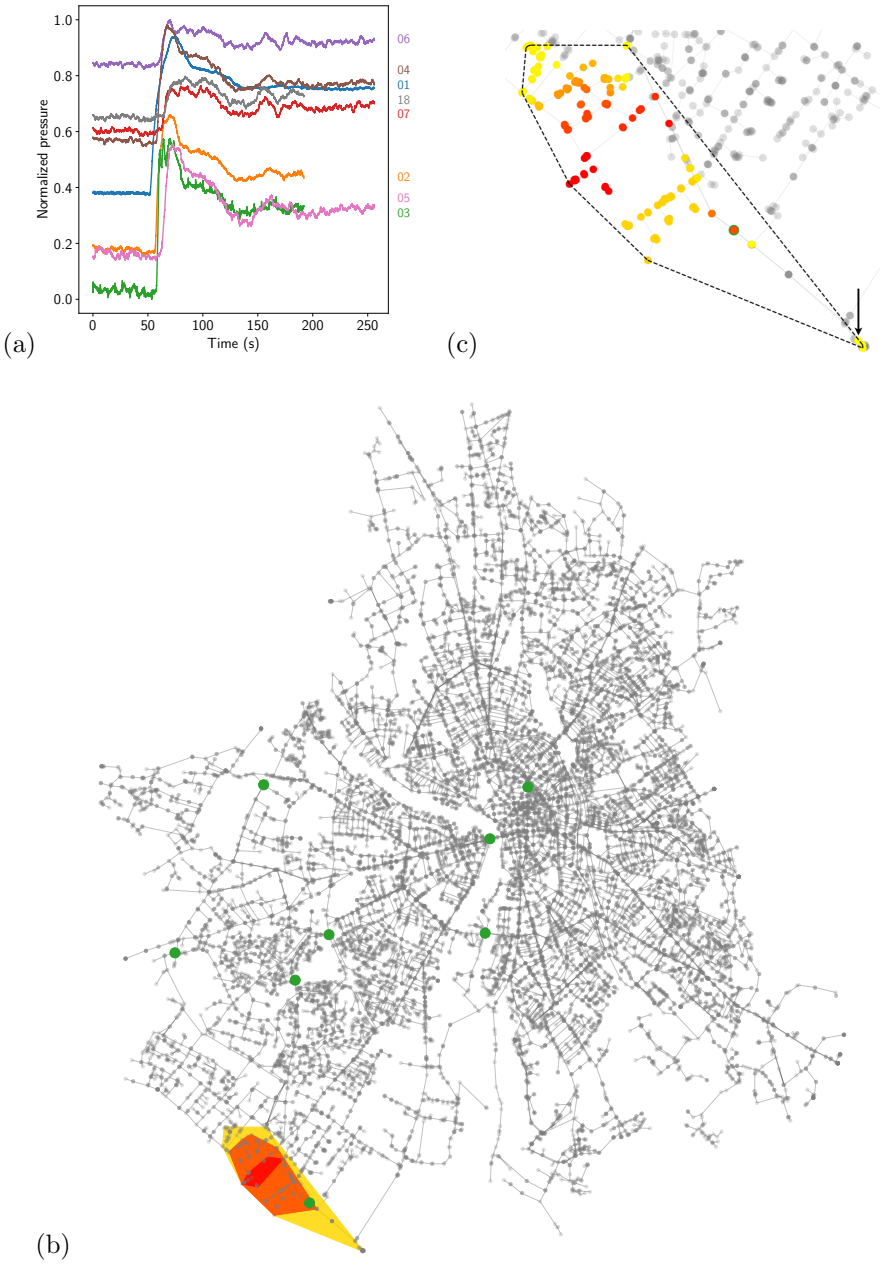

Figure 8: Same conventions as figure 7 for case 2.

Case #	% of pot. suc. source number	Hull area (%)	Pipe length (%)
Case 1	0.75	7.97	0.67
	0.5	7.27	0.40
	0.1	2.39	0.05
Case 2	0.75	15.92	0.77
	0.5	10.05	0.52
	0.1	4.24	0.08

Table 2: Hull areas (normalized by the total area of the network) and subgraph pipe lengths (normalized by the total pipe length of the network) versus the node proportion kept in the potentially successful source list for the real events illustrated in figure 7 and 8.

It decreases as the potentially successful source number used also levels ~~-~~ down. The proportion of pipe length within the convex ~~-~~ hull for the case 1 is also provided in table 2. It shows that (in the less selective choice) only 0.6% of the total pipe length ~~are~~ is worth of investigati~~oning~~ for finding the source. This shows that the methods already permit~~s~~ a huge screening over the total pipe length inside the network, a result of high operational interest. This is the geolocalized illustration of the method's *selectivity*. Figure 7c also provides a zoom into the ROI region ~~in order~~ to better visualize the convex ~~-~~ hull as well as the true source location. In the considered event, history matching has indeed permitted us to find the true location of the responsible event associated with a pipe breakage. The black arrow of figure 7c indicates that the breakage location indeed lies inside the ROI prediction of the method. This a posteriori confirmation is a supplementary demonstration that the proposed method is relevant for the field's water-hammer source identification.

Another geolocalization example associated with case 2 is illustrated in figure 8 for which the event responsible for the water-hammer wave has been identified as the start-up of one boost pump inside a drinking water production plant. In this case height detectors have been awakened (# $1, 2, 3, 4, 5, 6, 7, 18$) all showing a sudden uprising from base-state illustrated in figure 8a as opposed to the sudden depression found in figure 7a. This is indeed the expected behavior from a~~n~~ pressure injection event associated with a boost pump turn-on. The location of the pump is however found (figure 8c arrow) at the very edge of the ROI in this case. This might be related to the presence of high-diameter pipe connections of the drinking water production plant into the distribution system for which the associated wave velocity is perhaps roughly approximated. Concerning the quantitative figures obtained for the case 2 provided in table 2 a similar conclusion to case 1 can be raised. Also, in this case, the method~~s~~ permits a huge screening over the total pipe length worth investigating from the overall network.

4. Conclusions

This work has investigated the geolocalization of water-hammer events sources within a water distribution network from the use of high-frequency pressure detectors distributed within it. Combining first event detection with a time-reversal method, the *accuracy* and *selectivity* of the method have been analyzed within real network configurations, considering the very low density of pressure detectors. In this context, we demonstrate from a dedicated calibration procedure the relevance of the proposed method to perform a very good screening of potentially successful sources. The effect of noise either associated with the detector signal or the network uncertainty ~~have~~ has also been analyzed. Performance degradation of the method ~~have~~ has also been quantified for a noise range between 1 to 5% of the base signal. Finally, the relevance of the proposed method is illustrated in two field cases for which history-matching analysis provides a true source location consistent with the method's prediction.

Hence the proposed method has demonstrated the proof-of-concept that water-hammer events geolocalization ~~are~~ is possible with a combination of rather sparing computational and technological tools. Considering the possible managerial interest of such localization in insurance issues and/or repairing investigations, this contribution can lead to significant operational consequences ~~on~~ in the field.

~~Obviously,~~ Uncertainties ~~on~~ about the pipe's properties as well as network topological reliability could hamper a direct application of the method in some urban networks. Nevertheless, some more involved sensors and/or a more elaborated use of the signal beyond first-event detection might be interesting to develop in the future ~~in order~~ to partly overcome these uncertainties.

Declaration of Competing Interest

The authors have no competing interests to declare.

Acknowledgments

This work was supported by the collaborative ANRT Grant CIFRE 2019/1453 co-funded by SETOM, a dedicated society of Veolia for the public drinking water service of Toulouse Métropole operating under the brand Eau de Toulouse Métropole. The authors gratefully acknowledge F. Nospelle, from SETOM, for sharing his network knowledge and for his contribution in gathering the on-field information~~s~~ necessary to confirm the sources of the transient events herein analy~~sz~~ed.

Appendix. Local water-hammer wave velocity

Given the Young modulus E of the pipe, the Poisson coefficient ν_s, the pipe's density ρ_s, the dimensionless thickness $\alpha = e/R$ (e being the pipe thickness and R its radius), the acoustic water velocity c_0, K the

isothermal fluid bulk modulus, the water-hammer wave speed is given by

$$c = c_- \cdot c_p, \tag{.1}$$

with,

$$c_p^2 = \frac{c_0^2}{1 + \frac{2K}{\alpha E}\left(\frac{2(1-\nu_s^2)}{2+\alpha} + \alpha(1+\nu_s)\right)}. \tag{.2}$$

$$c_-^2 = \frac{1 + \mathcal{C}_s^2 + \frac{4\nu_s^2\mathcal{D}}{\alpha(2+\alpha)} - \sqrt{\left(1 + \mathcal{C}_s^2 + \frac{4\nu_s^2\mathcal{D}}{\alpha(2+\alpha)}\right)^2 - 4\mathcal{C}_s^2}}{2} \tag{.3}$$

with $\mathcal{C}_s = E/\rho_s c_p$ being the pulse wave velocity ratio, whilst $\mathcal{D} = \rho_f/\rho_s$ being the fluid to solid density one. These expressions can be found in Zhang et al. (1999); Tijsseling (2007).

References

Agathokleous A, Christodoulou S. Vulnerability of urban water distribution networks under intermittent water supply operations. Water Resour Manage 2016;30:4731–4750.

Caputo JG, Hamdi A, Knippel A. Inverse source problem in a forced network. Inverse Probl 2019;35(5):055006.

Che TC, Duan HF, Lee PJ. Transient wave-based methods for anomaly detection in fluid pipes: A review. Mech Syst Signal Process 2021;160. doi:10.1016/j.ymssp.2021.107874.

Ferrante M, Brunone B, Meniconi S. Leak detection in branched pipe systems coupling wavelet analysis and a Lagrangian model. J Water Supply Res T 2009;58(2):95–106. doi:10.2166/aqua.2009.022.

Grigoropoulos G, Ghidaoui MS, Louati M, Nasraoui S. Time reversal of waves in hydraulics: experimental and theoretical proof with applications. Journal of Hydraulic Research 2021;60(1):1–24.

Kessler A, Ostfeld A, Sinai G. Detecting accidental contaminations in municipal water networks. Journal of Water Resources Planning and Management 1998;124(4):192–8.

Meniconi S, Brunone B, Ferrante M, Capponi C, Carrettini C, Chiesa C, Segalini D, Lanfranchi E. Anomaly pre-localization in distribution-transmission mains by pump trip: Preliminary field tests in the Milan pipe system 2015;17:377. doi:10.2166/hydro.2014.038.

Meniconi S, Capponi C, Frisinghelli M, Brunone B. Leak detection in a real transmission main through transient tests: Deeds and misdeeds. Water Resources Research 2021;57(3):e2020WR027838.

Meniconi S, Maietta F, Alvisi S, Capponi C, Marsili V, Franchini M, Brunone B. Consumption change-induced transients in a water distribution network: Laboratory tests in a looped system. Water Resources Research 2022a;58(10):e2021WR031343.

Meniconi S, Maietta F, Alvisi S, Capponi C, Marsili V, Franchini M, Brunone B. A quick survey of the most vulnerable areas of a water distribution network due to transients generated in a service line: A lagrangian model based on laboratory tests. Water 2022b;14(17):2741.

Moosavian N, Lence B. Unified matrix frameworks for water hammer analysis in pipe networks. Int J Civ Eng 2020;18(11).

Nault JD, Karney BW, Jung BS. Generalized flexible method for simulating transient pipe network hydraulics. Journal of Hydraulic Engineering 2018;144(7):04018031.

Pal S, Hanmaiahgari PR, Karney BW. An overview of the numerical approaches to water hammer modelling: The ongoing quest for practical and accurate numerical approaches. Water 2021;13(11).

Plouraboué F, Uszes P, Guibert R. Source identification of propagating waves inside a network. IEEE Trans Netw Sci Eng 2022;9(3):1437–50.

Riaño-Briceño G, Sela L, Hodges BR. Distributed and vectorized method of characteristics for fast transient simulations in water distribution systems. Computer-Aided Civil and Infrastructure Engineering 2022;37(2):163–84.

Shen Z, Cao S, Wang WX, Di Z, Stanley HE. Locating the source of diffusion in complex networks by time-reversal backward spreading. Phys Rev E 2016;93:032301.

Shucksmith JD, Boxall JB, Staszewski WJ, Seth A, Beck SB. Onsite leak location in a pipe network by cepstrum analysis of pressure transients. J Water Supply Res T 2012;104(8):E457–65. doi:10.5942/jawwa.2012.104.0108.

Tijsseling A. Water hammer with fluid-structure interaction in thick-walled pipes 2007;85:844–51. doi:10.1016/j.compstruc.2007.01.008.

Truong C, Oudre L, Vayatis N. Selective review of offline change point detection methods. Signal Processing 2020;167:107299.

Wang R, Wang Z, Wang X, Yang H, Sun J. Pipe burst risk state assessment and classification based on water hammer analysis for water supply networks. Journal of Water Resources Planning and Management 2014;140(6):04014005.

Wang X, Camino GA, Che T, Ghidaoui MS. Factorized wave propagation model in tree-type pipe networks and its application to leak localization. Mech Syst Signal Process 2021;147:107116. doi:10.1016/j.ymssp.2020.107116.

Wang X, Ghidaoui MS. Pipeline leak detection using the matched-field processing method. Journal of Hydraulic Engineering 2018;144(6):04018030.

Wang X, Xie H. A review on applications of remote sensing and geographic information systems (gis) in water resources and flood risk management. Water 2018;10(5).

Zhang C, Zhang JJ, Ma CB, Korobkov GE. Algorithm for detecting multiple partial blockages in liquid pipelines by using inverse transient analysis. SPE 2021;26(3011–3039):1337–42.

Zhang L, Tijsseling A, Vardy E. FSI Analysis of Liquid-Filled Pipes. J Sound Vib 1999;224:69–99.